Monitoring of XRN4 targets reveals the importance of co-translational decay during Arabidopsis development

Marie-Christine Carpentier, Jean-Marc Deragon, Viviane Jean, Seng Hour Vichet Be, Cecile Bousquet-Antonelli, Rémy Merret

Short title: Co-translational decay dynamics across seedling development

Corresponding author: Rémy MERRET, email : remy.merret@univ-perp.fr, CNRS-LGDP UMR 5096, 58 av. Paul Alduy 66860 Perpignan, France

Article title: Monitoring of XRN4 targets reveals the importance of co-translational decay across Arabidopsis development

Authors: Marie-Christine CARPENTIER[1,2], Jean-Marc DERAGON[1,2,3] , Viviane JEAN[1,2], Seng Hour Vichet BE[1,2], Cécile BOUSQUET-ANTONELLI[1,2], Rémy MERRET[1,2]

[1]CNRS-LGDP UMR 5096, 58 avenue Paul Alduy 66860 Perpignan, France
[2]Université de Perpignan Via Domitia, LGDP-UMR5096, 58 avenue Paul Alduy, 66860 Perpignan, France
[3]IUF, Institut Universitaire de France, 75231 Paris Cedex 05, France

One sentence summary:

Co-translational decay mediated by XRN4 is dynamically regulated across Arabidopsis seedling development and fine-tunes translation efficiency.

List of authors contributions

R.M. designed and supervised the work. R.M conducted all the experiments present in this study. M.-C.C. conducted all the bioinformatic analysis. R.M. performed seedlings sampling with the help of V.J. R.M. performed western blotting with the help of S.H.V.B. R.M. wrote the manuscript, with the help of C.B.A and J.M.D.

Funding

This work was supported by the "Laboratoires d'Excellences (LABEX)" TULIP (ANR-10-LABX-41) to RM, by the "IUF Institut Universitaire Français" to JMD, by the ANR 3'modRN (ANR-15-CE12-0008) to CBA.

Email address of author for contact: remy.merret@univ-perp.fr

ABSTRACT

RNA turnover is a general process necessary to regulate proper mRNA amount at post-transcriptional level. Although long thought to be antagonistic to translation, the discovery of the 5'-3' co-translational mRNA decay demonstrated that both pathways can also be intertwined. This pathway globally shapes the transcriptome in different organisms and in response to stress. However, until now, the dynamic of this process in a growing organism was never assessed. In this study, we ran a multi-omic approach to reveal the global landscape of co-translational mRNA decay across Arabidopsis seedling development. We demonstrated that co-translational decay could be regulated by developmental cues. Using *xrn4-5* mutant, we demonstrated that XRN4 polyA$^+$ mRNA targets are mainly co-translational decay targets across development. As this pathway is tightly connected with translation, we also assessed its role in the control of translation efficiency. We discovered that clusters of transcripts could be specifically targeted by this pathway in a development-dependant manner to modulate their translation efficiency. Our approach allows the determination of a co-translational decay efficiency that could be an alternative to other methods to assess transcript translation efficiency. Thus, our results demonstrate the prevalence of co-translational mRNA decay in plant development and its role in translational control.

INTRODUCTION

Over its entire lifetime, any mature cytoplasmic mRNA is in balance between translation, storage and decay. This equilibrium maintains the proper dynamic of gene expression and is crucial to control mRNA homeostasis. Although long thought to be mutually exclusive, there is now a large body of evidence supporting that, in eukaryotes, mRNA translation and decay are interconnected (Heck and Wilusz, 2018). The impact of codon optimality on mRNA half-life is a clear example of this relationship. Codon optimality is defined as the ribosome decoding efficiency according to tRNAs availability. Genome-wide analyses revealed that yeast mRNAs enriched in optimal codons present high ribosome density and are more stable than mRNAs enriched in non-optimal codons (Presnyak et al., 2015). The finding that codon optimality is a key *cis* determinant of transcript stability places the ribosome as a core component linking translation elongation to mRNA degradation.

The most relevant interplay between translation and decay is the so called 5'-3' co-translational decay pathway where mRNAs are turned over while still engaged in polysomes and actively translated. This pathway first described in the yeast *Saccharomyces cerevisiae*, using reporter genes (Hu et al., 2009) was later on found to globally shape the polyadenylated transcriptome in yeast, mammalian cells and *Arabidopsis thaliana* (Pelechano et al., 2015; Yu et al., 2016; Tuck et al., 2020). For these mRNAs, decapping occurs on polysomes, allowing the 5'-3' exoribonuclease XRN1/4 to chase the last translating ribosome. The genome-wide effect of co-translational decay can be revealed by sequencing of RNA decay intermediates using high-throughput "degradome" approaches. All of them are based on the capture of 5' monophosphate decay intermediates including PARE (Parallel Analysis of RNA Ends, German et al., 2008), 5P-seq (5'P sequencing, Pelechano et al., 2015), Degradome-seq (Addo-Quaye et al., 2008) or GMUCT (Genome-wide Mapping of UnCapped Transcripts, Willmann et al., 2014). These approaches reveal that mRNA decay intermediates follow an XRN1/4-dependant, 3-nucleotide periodicity. This periodicity can be explained by the fact that XRN1/4 follows the last translating ribosome codon per codon, and since it is a processive enzyme, only degradation intermediates protected by ribosomes can be captured. Consequently, all these degradome approaches can not only give a snap-shot of co-translational mRNA degradation, but also reveal ribosome dynamics (Pelechano et al., 2015) and how degradation impacts this dynamic. As an example, in yeast, 5P-seq allowed the identification of general translation termination pauses, and novel codon-specific pausing

sites were detected, such as that at the rare proline codon CCG and at the arginine CGA codon (Pelechano et al., 2015). These additional pausings are explained by the lowest availability of corresponding tRNAs resulting in the slowing-down of the ribosome at these sites. Interestingly, these additional pausings were not detected in Arabidopsis flowers suggesting different ribosome dynamics in plants (Yu et al., 2016). Metagene degradome analyses also revealed 5'P reads accumulation 17 nucleotides upstream of stop codons (UAA, UAG and UGA). This distance corresponds exactly to a ribosome stalled at the A site. As termination step is slower than elongation, general 5'P reads accumulation can be revealed 17 nucleotides upstream of stop codons and can be used as a proxy of the transcriptome-wide co-translational decay activity. In addition, these approaches also unveil small RNA-guided cleavage sites (Franke et al., 2018), RNA-binding protein footprints (Hou et al., 2014), endonucleolytic cleavage sites (Anderson et al., 2018), exon junction complex footprints (Lee et al., 2020) and ribosome stalling sites (Hou et al., 2016). For example, degradome analysis in Arabidopsis revealed that AGO7 can bind to a noncleavable miR390 target site on the *TAS3* transcript leading to a ribosome stalling situation that was suggested to control translation of the *TAS3* gene (Hou et al., 2016). Ribosome stalling at uORFs (upstream Open Reading Frame) is another layer of translational control that can be detected by degradome data. For example, the stalling of 3 ribosomes can be detected on uORFs controlling Arabidopsis *BZIP3* main ORF translation (Hou et al., 2016).

At the physiological level, co-translational decay was shown to play important roles in the response to various stresses. In Arabidopsis, heat stress triggers 5'-ribosome pausing, the over accumulation of XRN4 in polysomes and the 5'-3' co-translational decay of around 1500 transcripts which code for proteins with hydrophobic N-termini (Merret et al., 2013, Merret et al., 2015). Recently, following stress, the yeast Lsm1-7/Pat1 complex was shown to trigger the co-translational decay of stress induced mRNAs limiting their translation and preventing an hyper-response (Garre et al., 2018). Consequently, defect in this pathway triggers the misregulation of translation inhibition under osmotic stress, which correlates with an abnormally high association of stress-induced mRNAs to active polysomes (Garre et al., 2018). Recently, this pathway was also proposed to be important for tubulin autoregulation (Lin et al., 2020). TTC5, a tetratricopeptide protein, recognizes tubulin nascent peptide and triggers the co-translational decay of its own transcripts to maintain proper tubulin homeostasis. TTC5 mutants abolished tubulin autoregulation and display chromosome segregation defects during mitosis. Taken together, these different examples support that co-

translational decay plays important roles in translation regulation under normal conditions and in response to different stresses. Nonetheless, if and how the co-translational decay process reshapes the transcriptomes and proteomes of cells across organism development remains unknown so far.

Transcripts can also be turned over through the cytosolic 5’ to 3’ decay pathway which takes place on ribosome free mRNAs. This so-called "general" 5' to 3' cytosolic mRNA turnover process takes place in three steps. Following poly(A) tail shortening (deadenylation), the VCS/DCP1/DCP2 decapping complex hydrolyses the mRNA cap structure. Then, the 5'-phosphate end of the decapped mRNA is attacked by the XRN1/4 exoribonuclease, which digests the body of the transcript. In Arabidopsis, XRN4 can target both deadenylated and polyadenylated fractions suggesting that part of the degradation could be deadenylation independent (Nagarajan et al., 2019). For co-translational mRNA decay, the importance of deadenylation is still unclear.

In Arabidopsis, at the whole organism level, the loss of XRN4 has minimal effects under normal growth conditions. Growth deficiencies were only reported in response to hormones or under stress conditions. Loss-of-function mutants of XRN4 are insensitive to ethylene (Potuschak et al., 2006) and hyper-sensitive to auxin and abscisic acid treatments (Wawer et al., 2018; Windels and Bucher, 2018). Recently, an *xrn4* mutant was found to be defective in the dark stress response and during nitrogen supply (Nagarajan et al., 2019). However, whether these deficiencies result from the failure of the general cytosolic or of the co-translational mRNA decay pathways (or a combination of both) is mainly unknown. Only one study distinguished both pathways and reported the exact role of co-translational decay in Arabidopsis heat stress response by analysing pools of mRNAs associated with ribosomes (Merret et al., 2015).

In the present study, we monitored the impact of co-translational decay across Arabidopsis seedling development. To do so, we assessed the genome-wide impact of XRN4 loss-of-function on polyA$^+$ mRNAs at the total, polysome and degradome levels. Through these approaches, we provide evidence that XRN4 mostly catalyzes polyadenylated mRNA degradation in polysomes. We also found that co-translational decay is dynamically modulated across development and can influence transcript translation efficiency, unveiling the importance of co-translational decay across plant development.

RESULTS

XRN4 differentially accumulates in polysomes across seedling development

To explore the hypothesis that translation and co-translational decay are regulated in response to developmental cues, we analyzed two read-outs (Figure 1). Firstly, the global translation activity was assessed by polysome quantification through sucrose density gradient on four developmental stages from 3 to 25-d old seedlings (Figure 1A). Considering that the cellular activity and hence the ribosome load per cell are most likely to be significantly different between developmental stages, we compared polysome contents from identical quantities of biomass rather than identical quantities of total RNA. Indeed, we observed that the polysome content is inversely correlated with the seedling age with the highest levels at 3 days, and a progressive decrease to reach a minimum at 25 days. Secondly, considering that XRN4 is the proposed main catalyzer of 5'-3' co-translational degradation (Merret et al., 2013; Yu et al., 2016), we used as read-out of this turnover activity, its accumulation in polysomes. We hence ran western blotting on input and polysomal fractions using XRN4 specific antibodies (Figure 1B). Although, detected at similar levels in all input fractions, XRN4 accumulation in polysomes differs across development. At 3-d-old, XRN4 is mostly absent from polysomes and progressively increases to reach a maximum at the 15-d-old stage a level globally maintained to 25-days (Figure 1B). These results suggest that co-translational decay activity could be regulated across seedling development.

Co-translational decay efficiency is regulated across seedling development

To identify XRN4 targets and get a deeper understanding of the dynamics of co-translational decay, we ran a multi-omic approach (Supplemental Figure 1). For each developmental stage, Col0 (wild type) and *xrn4-5* loss-of-function (SAIL_681_E01) seedlings were harvested in two biological replicates. As the loss of XRN4 has minimal effects under normal growth conditions, the observed differences between wild-type and mutant will be a direct consequence of the loss of XRN4 rather than a growth/developmental delay.

Each sample was used to purify: (i) total RNAs and (ii) RNAs associated to polysomes. Total RNAs were used on the one hand to run a polyA$^+$ RNA sequencing and on the other a degradome analysis through a GMUCT/RNA-seq approach. Briefly, GMUCT (also tagged as 5’P-seq) consists through the ligation of a 5’-RNA adapter in the capture and sequencing of polyA$^+$ mRNA molecules that carry a 5’-monophosphate. This also permits to counter select

mRNAs with a 5'-cap structure. Hence GMUCT allows to specifically sequence the population of mRNA molecules (full length and decay intermediates) that are in the course of being exonucleolytically degraded from their 5'-end following a decapping step or an endonucleolytic cleavage. Considering the very high processivity of 5'-exoribonucleases, only mRNAs with features slowing down the progression of the decay enzyme can be captured. Hence, GMUCT mostly to monitor the 5'-co-translational decay process, where the exoribonuclease digests the transcript chasing the elongating ribosomes. Polysomal RNAs were also purified through sucrose density gradient and sequenced following purification of the polyadenylated fraction (Supplemental Figure 1).

The total polyA$^+$ RNA-seq allows the capture of capped mRNAs free of ribosome, capped translated mRNAs and uncapped co-translational decay intermediates. The polysome polyA$^+$ RNA-seq allows the capture of both capped translating mRNAs and uncapped co-translational decay intermediates. The GMUCT approach captures uncapped co-translational decay intermediates (Supplemental Figure 1) hence permitting to monitor the cell 5'-degradome. For sequencing approach, the sequence of the biological repeats of each genotype displays a high reproducibility (R^2>0.94, Supplemental Table 1). Only transcripts with at least 1 RPKM/1RPM value in at least 1 library wild-type were kept for further analysis, leaving a total of 23,196 transcripts. Fold changes (FC) between *xrn4-5* and Col0 were calculated for each transcript at each developmental stage at total and polysome RNA levels (Figure 2, Supplemental Figure 2A-B). Using the DESeq2 pipeline (Love et al., 2014) and cut-off FCs above 2 or below 0.5, we identified mRNAs that differentially accumulate in the absence of XRN4 in the total and/or polysomal fractions (Figure 2). Considering that XRN4 is an RNA decay enzyme, we only focused on up-regulated mRNAs for further analyses. At the total RNA level, from 1 to 13 transcripts were identified as up-regulated in *xrn4-5* as compared to Col0 and at the polysome RNA level, from 0 to 23 transcripts were identified as up-regulated (Figure 2). From now on, the pool of mis-regulated transcripts will be referred to as differentially expressed (DEGs). These data are consistent with previous analyses showing that under normal conditions, only a handful of XRN4 targets can be identified at the total and polysomal polyA$^+$ RNA level (Merret et al., 2015).

As our main goal in this study is to determine the prevalence of co-translational 5'-3' mRNA decay across development, we focused on degradome data. The two main features of co-translational decay are the accumulation of the 17 nt long ribosome footprint at the translation

termination site and the 3-nucleotide periodicity of fragments resulting from the degradation of mRNA open reading frames (Pelechano et al., 2015; Yu et al., 2016). To assess the reliability of our analysis, a metagene analysis of the 5'P reads obtained by GMUCT was performed around stop codons at each developmental stage (Figure 3A-D). The relative abundance of reads at each position relative to the stop codon was determined. At all stages, a clear 3-nt periodicity pattern is observed as previously described (Yu et al., 2016). Additionally, a clear over-accumulation of reads 17 nt before stop codons is also detected. This accumulation corresponds precisely to the 5′ boundary of the ribosome with its A site stalled at a stop codon. Interestingly, a differential accumulation at this position is observed across development reaching its maximum at 15-d-old stage (Figure 3C), suggesting that the activity of the co-translational decay pathway could be controlled through development. Moreover, at 7-d and 15-d-old stages, an additional peak is observed 47 nt before stop codons (Figure 3B-C). A similar phenomenon was previously observed in yeast (Pelechano et al., 2015) but was not detected in Arabidopsis flowers (Yu et al., 2016). It corresponds to two ribosomes stalled at stop codons as the distance between the two peaks (30 nt) exactly matches one ribosome footprint. To determine if additional peak(s) could also result from a ribosome stalling at sub-optimal codon(s), we looked for possible enrichment of 5'P read ends in coding regions other than the ones surrounding stop codons (Supplemental Figure 3). We could not identify additional peaks at any codon, other than stop codons, in our four tested developmental conditions. Thus, in our experimental conditions, we find no evidence for ribosome stalling at sub-optimal codons. This also confirms that the -47 nt peak, only observed in developmental stages where the co-translational decay rate is highest, is not associated with a slowing down of ribosome at a specific codon but represents the footprint of two ribosomes stalled at stop codons. Taken together, these observations support that co-translational decay activity is regulated across development.

Next, we performed the same analysis using *xrn4-5* degradome data (Figure 3E-H). For all developmental stages, a decrease in reads accumulation at -17 nt before stop codons is observed, suggesting that the co-translational decay pathway is severely impaired in this mutant and supporting the main role of XRN4 in this pathway. To identify XRN4 co-translational decay targets, we used the DESeq2 pipeline on Col0 and *xrn4-5* degradome data (Supplemental Figure 2A-B) and compared the FCs across development. For all the differentially accumulated targets, the median fold change is systematically higher than 2.5 with a maximum at 3-days (Supplemental Figure 4A). To extract the most significant targets,

a cut-off FC above 2 was applied. While in total and polysome RNA data, only a handful of XRN4 targets were identified, the degradome data identifies several hundreds of mis-regulated mRNAs (Figure 4A-D). And consistently with XRN4 function as decay enzyme, 98% of differentially expressed genes are up-regulated. The number of co-translational decay targets increases across development reaching it maximum at 15-days (479) before dropping again at 25-days (152). The differential accumulation of 5'P read ends at 17 nt before stop codon suggests that the repertoire of co-translational decay targets and/or their decay rates are developmentally regulated. To test this hypothesis, we performed a Venn diagram on lists of transcripts up-regulated in the *xrn4-5* in degradome data (Figure 4E, Supplemental Table 2). A total of 565 unique targets were identified with only 47 targets shared by all stages. Each stage presents specific targets with 25, 18, 253 and 37 mRNAs more sensitive to co-translational decay at 3-, 7-, 15- and 25-d-old stages respectively. Additionally, close developmental stages share more targets than more distant one. As an example, except for the 47 common targets, 65 common targets were identified between 25- and 15-d-old stages whereas 3 targets are shared between the 25 and 3-d-old stages (Figure 4E). In order to determine biological processes targeted by co-translational decay, a GO analysis was performed on transcripts identified as up-regulated in *xrn4-5* in degradome data at all developmental stages. A clustering approach was performed using DAVID software (Supplemental Table 3). "Redox signalling" processes are mainly affected by XRN4 at 3-d-old stage. "Auxin/Growth", "Response to stress" and "DNA binding" processes are preferentially affected at 7-d-old stage compared to "Ribosome/translation", "DNA binding" and "RNA binding" processes that are affected at 15-d-old stage (Supplemental Table 3). At 25 days, these same GO terms as for the 15-d-old stage are represented but with a lower enrichment score.

Next, we reasoned that genes we find up-regulated in the absence of XRN4 in our degradome data, should show an augmented half-life when the 5'-3' decay system is impaired. VARICOSE (VCS) is part of the decapping holoenzyme DCP1/DCP2/VCS and the DEAD box RNA helicases RH6, 8 and 12 were recently identified as co-factors of the 5'-3' cytoplasmic mRNA turnover (Sorenson et al., 2018; Chantarachot et al., 2020). We hence used data from these two recent articles that report genome-wide, mRNA half-lives in wild-type and *vcs-7* or *rh6812* loss-of-function mutants. Of the 565 mRNAs we find up-regulated in *xrn4-5*, 444 (>78%) are detected in the Sorenson dataset, of which 85% have a half-life below 240 min (Figure 4F, Supplemental Table 2, Col0 data). Consistently, 77 % of the 390

of our co-translational decay targets that are present in the Chantarachot data, also show half-lives below 240 min (Figure 4G, Supplemental Table 2, Col0). This first observation supports that most of the transcripts that are degraded co-translationally from 5', are intrinsically short-lived. Next, we observed that in the absence of an active decapping enzyme (*vcs-7* mutant) or in a background without cofactors of the 5'-3' decay (*rh6812* mutant), their half-lives significantly increase (Figure 4F, compared the Col0 to *vcs-7* boxplot, Figure 4G compare the Col0 boxplot to the *rh6812* one). Furthermore, the Sorenson data suggest that these mRNAs are mostly decayed through a 5'-3' process. Indeed, mRNAs can be decayed either from 5', following decapping and/or from 3' either by the exosome complex or by the 3'-5' exoribonuclease, SOV. In addition, mRNAs that are not naturally decayed from 5'- can be turned down by this pathway in the absence of functional exosome or VCS enzymes. The Col0 ecotype was found previously to carry a *sov*-defective allele (Zhang et al., 2010), hence to ascertain that mRNAs up-regulated in the *vcs-7* background are natural targets of the 5'-pathway, Sorenson et al. also used Col0 Arabidopsis complemented with a functional allele of *SOV*. mRNAs we find up-regulated in the absence of XRN4 here again show increased half-lives in the absence of VCS despite the presence of an active SOV (Figure 4F compared Col0 to *vcs-7* SOV^{LER}). This increase is not seen when VCS is active such as in Col0 SOV^{LER} (Figure 4F compared Col0 to Col0 SOV^{LER}). This further supports that XRN4 co-translational decay targets are actual and specific targets of the 5'-3' degradation pathway.

A key question is how the 5'-3' decay pathway and more specifically how the 5'-co-translational degradation process recognizes its targets amongst the whole cell transcriptome. We hence looked for putative *cis* elements shared by mRNAs we found as XRN4 co-translational decay targets. To do so we retrieved the 5' and 3'-UTRs, the CDS sequences of all targets, and looked for common features as compared to a random set of transcripts non-targeted by XRN4. Although, no differences were found in 5'UTR and 3'UTR lengths, a significant reduction in intron number and CDS length was observed for XRN4 co-translational decay targets (Figure 4H-I, Supplemental Figure 4B-C). In addition, AU-motifs were found enriched in their 5'UTR (Figure 4J). This observation is consistent with previous study showing that short-lived mRNAs have less introns and AU-rich motifs in their 5'-UTRs (Narsai et al., 2007; Sorenson et al., 2018). All together, these data suggest that *trans* and *cis* elements could regulate co-translational decay activity.

Co-translational decay activity across development can influence translation efficiency

Hence our above results suggest that co-translational decay specificity and efficiency is regulated in response to developmental cues. We next wondered about the molecular role of this regulation. Since co-translational decay and translation are interrelated, we asked whether the former could control protein production. We rationalized that, for a given mRNA, a co-translational decay rate higher than the translation rate should result in a decrease in translation efficiency and *vice-versa*. To explore this, we compared variations across development at polysome and degradome levels in Col0 background (Figure 5A). To limit variations at polysome and degradome levels, we focused our analysis on transcripts detected (RPKM>1 in all libraries) and remaining stable across development at the total RNA level (e.g. fold change between 0.66 and 1.5 between all conditions) resulting in 3,366 mRNAs (Supplemental Figure 2C). For these transcripts, variations at polysome RNA levels were compared to that at the degradome level. Values were normalized to the 3-d-old stage and the dynamic was assessed across development (Figure 5A and 5B). Interestingly, based on p-values, the median variation of the degradome values appears more dynamic across development than that of the polysomal values. To test this, we calculated the ratio between degradome and polysome values for each mRNA (Supplemental Figure 2C). We called this ratio "co-translational decay efficiency" as it reflects the proportion of polysome associated with uncapped mRNA decay intermediates (degradome data) compared to the total amount (capped and uncapped) of polysome-associated mRNAs (polysome data). A high ratio would suggest a high co-translational decay activity resulting in a low translation efficiency compared to a low ratio suggesting a high translation efficiency. A heat map was generated to observe the variation of this efficiency across development (Figure 5C). Interestingly, this efficiency varies between transcripts and is highly modulated across development. Six good resolution clusters were obtained, the behavior of which can be monitored across development. Transcripts from cluster 1 were highly targeted by co-translational decay at 15-d-old stage while those from cluster 5 are mostly targeted at the 3-d-old stage. Cluster 3 was also remarkable as it is formed with mRNAs that are progressively targeted by the co-translational decay until the 25-d-old stage. As our hypothesis is that co-translational decay could influence translation efficiency, we set to monitor level variations across development of two proteins LUT1 and CDC2 that belong to cluster 2 and 3 respectively. These mRNAs were selected as case studies because they show important variations of their co-translational efficiency that are mostly due to variations of their degradome values with stable quantities in total and polysomal fractions across development (Supplemental Figure 5). Western blotting shows that LUT1 levels are highest at 3-d-old stage and decrease at 7-d-old and 15-d-old

stages where its transcript's co-translational decay efficiency is highest. At 25-d-old stage, *LUT1* degradome value decreases and consistently its protein levels increase as compared to 7 and 15-day (Figure 5D, Supplemental Figure 5). In contrast, CDC2 was mostly detected at 3-d-old stage which is consistent with its low co-translational decay efficiency at this stage (Figure 5E, Supplemental Figure 5). Protein level variations are the consequence of both production (translation) and decay rates variations, hence steady-state western blotting is not the most accurate read-out of translation efficiency. Nonetheless, with the LUT1 and CDC2 cases we observe a perfect correlation between co-translational efficiency and steady-state protein levels (Figure 5D and E) supporting that indeed co-translational decay could be a mean to fine-tune translation.

DISCUSSION

The major objective of this study was to monitor the dynamics of co-translational decay across Arabidopsis seedling development. Using a multifaceted genome-wide approach, we provide evidence that co-translational decay is highly modulated across development with a maximum at 15-d-old stage. Using the *xrn4-5* loss-of-function mutant (Souret et al., 2004; Merret et al., 2013), we find that the majority of co-translational mRNA decay in seedling is catalyzed by XRN4, as previously proposed in flower tissue (Yu et al., 2016). However, as the 3-nt periodicity is maintained in *xrn4-5*, as well as a low level of 17 nt 5'P reads before stop codons, other 5' to 3' exoribonucleases must be involved in this process. In yeast, the nuclear Xrn (Xrn2p) was proposed to relocalize to the cytoplasm of *xrn1-null* mutant and restore cytosolic mRNA turnover (Johnson, 1997). However, since Arabidopsis has not one but two nuclear 5 to 3' exonucleases (XRN2 and 3) and since the *xrn3* loss-of-function mutant is lethal (Gy et al., 2007), the hypothesis of nuclear XRNs complementing a deficient cytosolic enzyme is challenging to assess.

The polysome fraction was until recently considered to be composed essentially of actively translating mRNAs and was routinely used to assess mRNA translation efficiency after normalization to total RNA levels (see an example in Bai et al., 2017). The discovery of the co-translational decay and its conservation in evolutionary distant eukaryotes (Hu et al., 2009; Hu et al., 2010; Hou et al., 2016; Yu et al., 2016; Simms et al., 2017; Ibrahim et al., 2018), suggests that the proportion of actively translated mRNAs in polysomes might be much lower than initially expected. Translation efficiency is often assessed by ribosome profiling (Ingolia

et al., 2009) or TRAP (Translating Ribosome Affinity Purification, Reynoso et al., 2015). But these approaches do not take into account the fact that part of mRNAs attached to the ribosomes might be undergoing a degradation. Thus, these approaches can give rise to misleading conclusions. In yeast, 5′P decay intermediates represent more than 12% of the polyA$^+$ mRNA fraction (Pelechano et al., 2015). In our study, we found that at least 3,366 transcripts present variations in degradome data across development and that their co-translational decay rate could be an efficient way to the cell to control their translation efficiency (Figure 5). Thus, to take into account the co-translational decay in translation efficiency measurements, we calculated the ratio between degradome and polysome values for each transcript as proxy (Figure 5C). This ratio can be determined for each transcript and compared pairwise between conditions or genetic backgrounds. A high ratio would suggest a low translation efficiency and conversely. As a proof of concept, we monitored protein accumulation of the LUT1 and CDC2 genes and found that protein levels vary in an inversely proportional manner to this ratio in both cases (Figure 5, Supplemental Figure 5). We hence propose to use this ratio as an additional way to determine transcript translation efficiency. We also posit that it would be a more accurate read-out than the mere ratio between polysomal and total mRNA levels. The determination of this efficiency will be crucial under conditions where co-translational decay is highly modulated such as development or stress exposure (Merret et al., 2015; Garre et al., 2018).

In addition to its role in translation efficiency modulation, our analysis allows the identification of specific XRN4 co-translational decay targets (Figure 4). In a landscape analysis of Arabidopsis mRNA half-lives, the authors found that short half-lived mRNAs targeted by decapping and 5'-3' degradation present less introns that stable ones (Sorenson et al., 2018). Consistently, this feature is shared by transcripts targeted by co-transcriptional decay in our analysis (Figure 4H, Supplemental Table 2). Co-translational decay targets are also enriched in AU-motifs in their 5'-UTRs, a motif also known to be shared by unstable transcripts (Narsai et al., 2007). A low intron complexity and the presence of AU-rich motifs could be some of the *cis* determinants of co-translational target recognition. Additionally, we found that the mRNA half-life range of XRN4 co-translational decay targets increases in mutants involved in 5'-3' decapping dependant decay such as *vcs-7* and *rh6812*, key factors of decapping activity (Figure 4F-G). The higher stability of these transcripts in these mutants is consistent as decapping is a necessary and crucial step for XRN4 activity. Interestingly, in yeast DHH1, homologue of RH6, 8 and 12 was proposed to couple mRNA translation to

decay (Radhakrishnan et al., 2016). These findings could support that VCS, RH6, 8 and 12 could be *trans* determinants of co-translational target recognition as recently discussed (Merret and Bousquet-Antonelli, 2020).

Analysis of enriched GO terms associated with co-translational decay targets reveals six major GO terms ("Auxin/Growth", "Response to stress", "DNA binding", "Ribosome/translation", "RNA binding" and "Redox signalling"). Published PARE data identified similar GO terms such as "mRNA processing" or "Ribosome biogenesis" shared by polyadenylated targets of XRN4 (Nagarajan et al., 2019). Recently, it was proposed that XRN4 contributes to root growth under normal conditions and upon salt stress by an unknown mechanism (Kawa et al., 2020). Interestingly, in "auxin/growth" GO term, we identified many genes targeted by the co-translational decay pathway that are associated with growth regulation (such as "response to auxin" GO:0009733, Supplemental Table 3) consistently with the described role of XRN4 in root development. As an example, *RVE2* (At5g37260), a gene involved in lateral root formation and a VCS substrate (Supplemental Table S16 of Kawa et al., 2020), was identified as a co-translational target of XRN4 at 7 days (Supplemental Table 3). While in these different studies, the respective contributions of both 5'-3' cytosolic and co-translational decay was not addressed, our results suggest that at least part of these XRN4 targets could be decayed co-translationally

Co-translational decay is an evolutionarily conserved mechanism found in many organisms such as yeast (Pelechano et al., 2015), Arabidopsis (Yu et al., 2016), Soybean (Hou et al., 2016), Barley (Hou et al., 2016), and mammalian cells (Tuck et al., 2020). This pathway was described as being involved in different stress responses (Merret et al., 2015; Pelechano et al., 2015; Garre et al.; 2018). But until now, analyses were only focused on stable lines or specific tissues. Our data demonstrate that the 5'-co-translational decay is dynamically modulated across development and important for proper regulation of protein expression and suggest that this pathway could be important for plant development and physiology.

MATERIAL AND METHODS

Growth conditions

Analyses were carried out with Columbia-0 line as wild type and *xrn4-5* mutant (SAIL_681_E01). Plantlets were grown on synthetic Murashige and Skoog medium (Duchefa) containing 1% Sucrose and 0.8% plant agar at 22°C under a 16-h-light/8-h-dark regime. Same growth conditions were applied for soil culture.

Sampling procedure for RNA sequencing

To generate two biological replicates, two distinct batches of seeds (generated from different parent plant) were used for each genotype. All samples were generated at the same time as follows. Seeds were sown *in vitro* on 20 square plates for each replicate and genotype. After 3 days, plantlets from 6 plates were pooled and harvested to generate 3-day samples. The same procedure was performed at 7 days and 15 days to generate 7- and 15-day samples respectively. Plantlets from the 2 remaining plates were transferred to soil for an additional 10 days to obtain 25 day-samples. In this case, the rosette and the primary root were collected. For each developmental stage, at least 10 plantlets were pooled to avoid individual-specific bias.

Polysome profile analysis

Polysome profiles were performed as described previously (Merret et al., 2013). In brief, 400 mg of tissue powder were homogenized with 1.2 mL of lysis buffer (200 mM Tris-HCl, pH 9.0, 200 mm KCl, 25 mM EGTA, 35 mM $MgCl_2$, 1% detergent mix [1% Tween 20, 1% Triton, 1% Brij35, and 1% Igepal], 1% sodium deoxycholate, 0.5% polyoxyethylene tridecyl ether, 5 mM DTT, 50 $\mu g.mL^{-1}$ cycloheximide, 50 $\mu g.mL^{-1}$ chloramphenicol, and 1% protease inhibitor cocktail [Sigma-Aldrich]). Crude extract was incubated 10 min on ice. After centrifugation, nine hundred microliters of crude extract was loaded on a 15% to 60% Sucrose gradient (9 mL). Ultracentrifugation was performed with an SW41 rotor at 38 000 for 3 h. Polysome profile analyses were performed with an ISCO absorbance detector at 254 nm. Twelve fractions of 650 µL were collected. Proteins were extracted from fractions 6 to 12 (corresponding to polysomes). 2 volumes of absolute ethanol were added for each fraction. Proteins were precipitated 6 hours at 4°C before centrifugation. Pellets were washed and resuspended in 10 µL of Laemmli 4X. For polysomal RNA, extraction was performed as in Merret et al., 2015 using Monarch Total RNA Miniprep Kit (New England Biolabs).

Total RNA extraction

Total RNA was extracted using Monarch Total RNA Miniprep Kit (New England Biolabs). RNA quality was assessed using Agilent RNA 6000 Nano kit (Agilent).

RNA library preparation

RNA library preparation was performed on total or polysomal RNA using NEBNext® Poly(A) mRNA Magnetic Isolation Module and NEBNext Ultra II Directional RNA Library Prep Kit (New England Biolabs) according to manufacturer's instructions with 1 µg of RNA as starting point.

GMUCT assay

GMUCT library was prepared as described previously with slight modifications (Willmann et al., 2014). Briefly, 50 µg of total RNA were subjected to two polyA$^+$ purification. After 5'adapter ligation, excess of adapter was removed by a new round of polyA$^+$ purification. Reverse transcription was performed using Superscript IV system with manufacturer's instructions. cDNAs were amplified with 11 cycles of PCR. Libraries were purified using SPRIselect beads prior to quality control and normalization.

RNA sequencing

Libraries quality was checked using Agilent High Sensitivity DNA kit (Agilent). Libraries were normalized, multiplexed and sequenced on NextSeq 550 (Illumina) in single-reads 75 pb.

Bioinformatic analysis

For total and polysome RNA libraries, after filtering out reads corresponding to chloroplastic, mitochondrial, ribosomal and small RNA sequences using bowtie2, reads were mapped against TAIR10 genome using Hisat2 and the gtf TAIR10 annotation file with standard parameters. Reads count by gene was performed by Cufflinks in RPKM (reads per kilobase by millions mapped reads). For GMUCT analyses, reads were trimmed to 50 pb using Trimmomatic prior to mapping. Reads count was performed using bedcoverage from Bedtools suite and normalized by total of mapped reads (read per millions, RPM). For 5'P reads abundance, the bam file was converted into bed file containing only the first nucleotide of each read. Differential expression analyses were performed using Biocunductor R package

DESeq2, with an FDR of 0.05. P-values were corrected for the multiple tests by Benjamin-Hochberg rule (adjusted p-value). Analysis of codon enrichment was performed as previously described (Yu et al., 2016). For Notched plot analysis, Shapiro test was applied to test normality of the dataset. Then nonparametric Wilcoxon test was performed between each developmental stage. GO analysis was performed using DAVID software (Huang et al., 2009) with default settings, the six major clusters were retained for analysis. For mRNA features analysis, UTRs, introns and CDS sequences were obtained from Araport11 database and are listed on Supplemental Table 2. RNA half-lives data were collected from Dataset_S2 of Sorenson et al., 2018 (Columns "alpha_WT", "alpha_*sov*", "alpha_*vcs*", "alpha_*vcs sov*") and from Supplementary Table S4 of Chantarachot et al., 2020 (Columns mRNA Half-life "WT_Col-0" and "*rh6812*") and are presented on Supplemental Table 2. Only transcripts present in each dataset were kept for statistical analysis. A Wilcoxon test was systematically performed to test significance (presented on Supplemental Table 5).

Western blot

After electrophoretic separation by SDS-PAGE gels, proteins were electrotransferred on polyvinylidene fluoride membranes. Immunoblottings were performed in TBS-5% skimmed milk-1% Tween. Primary antibody was incubated overnight at 4°C under constant agitation. After incubation, membranes were washed 6 times with TBS-1% Tween. A horseradish peroxidase-coupled secondary antibody was incubated in TBS-5% skimmed milk- 1% Tween 45 minutes at room temperature. Membranes were again washed 6 times with TBS-1% Tween and revealed with the Immobilon-P kit from Millipore. Image acquisition was performed using Fusion FX imaging system (Vilber). Antibodies against XRN4 (Merret et al., 2013), LUT1 (Agrisera), CDC2 (Agrisera), UGPase (Agrisera) and RPL13 (Merret et al., 2013) were utilized at 1/1,000th, 1/1,000th and 1/3,000th, 1/5,000th and 1/100,000th respectively.

Accession numbers

The accession numbers for the RNA-seq data reported in this article are NCBI Bioprojects PRJNA604882 for total RNA data, PRJNA604883 for polysome RNA data and PRJNA604884 for GMUCT data.

Acknowledgments

We thank Drs. Xiang YU and Brian GREGORY (University of Pennsylvania) for advices on GMUCT bioinformatic analysis. We also thank the sequencing facility of Perpignan University Via Domitia BioEnvironnement platform (Perpignan, France).

559 **FIGURES LEGENDS**

560

561 **Figure 1 : XRN4 differentially accumulates in polysomes across seedling development.**
562 **A.** Polysomal extracts prepared from 3-, 7-, 15- and 25-d-old seedlings were fractionated on a
563 sucrose gradient and polysome traces obtained through measurement of OD_{254nm}. Polysome
564 profiling were performed starting from identical quantities of N_2-pulverized tissues (e.g 300
565 mg of biomass). **B.** Total proteins extracted from polysomal and input fractions were analyzed
566 by western blotting. The four blots were probed with an antibody specific to XRN4. Inputs
567 correspond to an equivalent of 10 mg of tissue powder for all stages. For polysomal fraction,
568 loaded proteins were precipitated from identical volumes of each fraction. Data are
569 representative of at least three replicates.

570

571 **Figure 2 : XRN4 loss-of-function has low impact across seedling development at total**
572 **(A) and polysome (B) RNA levels.** Fold changes between *xrn4-5* and Col0 (wt) were
573 calculated for each transcript in each condition. The $\log_2$ value of the mean is represented in
574 each graph. The number of transcripts significantly regulated in *xrn4-5* is reported (as DEG in
575 red for up-regulated and grey for down-regulated transcripts) and was calculated using
576 DESeq2. Dashed red lines mark the $|\log_2(2)|$ values.

577

578 **Figure 3 : Metagene analyses displaying the abundance of 5'P reads relative to stop**
579 **codons. A.** wt 3-d-old stage, **B.** wt 7-d-old stage, **C.** wt 15-d-old stage, **D.** wt 25-d-old stage,
580 **E.** *xrn4-5* 3-d-old stage, **F.** *xrn4-5* 7-d-old stage, **G.** *xrn4-5* 15-d-old stage, **H.** *xrn4-5* 25-d-old
581 stage. Mean ± SD. The illustrations represent 5'P intermediates accumulation at - 47 nt and -
582 17 nt before stop codons.

583

584 **Figure 4 : Identification and features of XRN4 co-translational decay targets across**
585 **development. A-D.** Volcano plot of the change in read abundance in *xrn4-5* over wt (Col0).
586 Vertical red dotted lines mark the $|\log_2(2)|$ values. Log_2 fold change and Benjamini-Hochberg
587 adjusted p-values (BH) were calculated through the DESeq2 pipeline (as DEG in blue for up-
588 regulated and red for down-regulated transcripts). Horizontal plain black lines demarcate
589 adjusted p-values of 0.05. **E.** Venn diagram of co-translational decay targets across
590 development. **F-G.** Majority of XRN4 co-translational decay targets show longer RNA half-
591 life in *vcs-7, vcs-7* SOV^{LER} mutants (F) and *rh6812* mutant (G). RNA half-lives were
592 collected from Sorenson et al., 2019 (F) or from Chantarachot et al., 2020 (G). Only

transcripts present in each dataset are represented (N = 444/565 for F or N = 390/565 for G). **H-J.** Introns number, CDS length, and proportion of AU-motif in 5'UTR respectively of transcripts targeted by XRN4 compared to non-targeted random transcripts. N=565. *** p-values < 0.001, * p-values < 0.05, n.s. non significant.

Figure 5: Co-translational decay is regulated across development and influences protein production. A. Transcript variation at polysome level across development using 3-days as a reference (N=3,366). **B.** Transcript variation at degradome level across development using 3-days as a reference (N=3,366). Gray lines represent individual transcript variation. Transcript distribution is represented by notched boxplots and significance was assessed by p-values (nonparametric Wilcoxon test). **C.** Heat Map of co-translational decay efficiency (ratio in degradome data over polysome RNAseq data) (N=3,366). Red values correspond to a high decay efficiency and yellow values to a low decay efficiency. **D, E.** Western blottings using LUT1 and CDC2 antibodies respectively. Both candidates were analyzed on distinct SDS-PAGE gels (8% and 10% acrylamide respectively). RPL13 and UGPase antibodies were used as loading controls. Each western blot was performed on two biological replicates**.**

SUPPLEMENTAL DATA

Supplemental Figure 1 : Representation of the experimental procedure. A. To generate two biological replicates, two independent batches of seeds were used for each genotype. A time-course sampling was performed to harvest 3-d-old, 7-d-old, 15-d-old and 25-d-old seedlings in two biological replicates. Col0 (wt) and *xrn4-5* (SAIL_681_E01) were used in this study. **B.** On each sample, total RNA extractions were performed to determine the transcriptome and the degradome through RNA sequencing and GMUCT approaches respectively. From the same biological samples, polysomes were purified through fractionation of sucrose density gradients and their levels determined through measurement of OD_{254nm} in each fraction. Polysomes traces were recorded and polyadenylated RNAs were purified from pooled fractions containing polysomes (translating ribosomes). The total $polyA^+$ RNAseq allows the capture of capped free mRNAs, capped translated mRNAs and uncapped co-translational decay intermediates. The polysome $polyA^+$ RNAseq allows the capture of capped translating mRNAs and uncapped co-translational decay intermediates. The degradome allows the capture of uncapped co-translational decay intermediates.

Supplemental Figure 2 : Representation of the bioinformatic analysis. A. For each library, reads were mapped against TAIR10 genome using Hisat2. Then, transcripts quantification was performed using Cufflinks for total and polysome libraries (RPKM) and using Bedcoverage for degradome libraries (RPM). **B.** To identify XRN4 targets, transcripts with a least 1 RPKM/RPM in 1 library were kept (N=23,196). Then, a fold change (FC) analysis was performed between *xrn4.5* and Col0. Biological replicates were analyzed separately and differential expression analysis was performed using DESeq2 to determine significant targets. A FC of 2 and a FDR of 0.05 were applied as criteria to identify XRN4 targets. **C.** To determine co-translational decay efficiency, transcripts with a least 1 RPKM/RPM in all libraries were kept (N=13,333). Then, transcripts remaining stable across development at the total RNA level (e.g. fold change between 0.66 and 1.5 between all conditions) were kept (N=3,366). Finally, the co-translational decay efficiency (ratio between degradome and polysome values for each transcripts) in Col0 was determined.

Supplemental Figure 3 : Enrichment of 5′P read ends at the ribosome boundary of mRNA along mRNA coding regions. Red dots denote codons with significant enrichment of 5′P read ends at their ribosome boundary sites, while dark dots denote codons that are not significant for this value. The "stop" red dot represents the mean value of the three stop codons. Significance was assessed using a $\chi 2$ test.

Supplemental Figure 4 : A. Boxplots of the range of fold change in *xrn4* mutant compared to wt for differentially expressed transcripts in degradome data identified at 3-, 7-, 15- and 25-days respectively. Numbers of transcripts and median of fold change are indicated. Red dashed line represents a FC of 2. **B-C.** Distribution of 5'UTR length or 3'UTR length of XRN4 co-translational targets *versus* XRN4 non-targets. N=565, n.s. non significant.

Supplemental Figure 5 : Values obtained for LUT1 and CDC2 transcripts at TOTAL, POLYSOME and DEGRADOME levels in RNAseq data. Data were extracted from Supplemental Table 1. Mean ± SD. Western blot of a second replicate is also presented.

Supplemental Table 1 : Differential expression analysis of 23,196 genes by DEseq2 of TOTAL, POLYSOME and DEGRADOME mRNA-seq data associated with Figures 2 and 4.

Supplemental Table 2 : List 565 XRN4 co-transcriptional decay targets identified across development using DEseq2 associated with Figure 4.

Supplemental Table 3 : Enriched GO terms associated with XRN4 co-translational decay targets across development

Supplemental Table 4 : Variation of co-translational decay efficiency of 3,366 genes stables at TOTAL RNA level across development associated with Figure 5

Supplemental Table 5 : Results of statistical analysis used in this manuscript

671 LITERATURE CITED

672

673 **Addo-Quaye C, Eshoo TW, Bartel DP, Axtell MJ** (2008) Endogenous siRNA and miRNA
674 Targets Identified by Sequencing of the Arabidopsis Degradome. Curr Biol **18**: 758–762
675 **Anderson SJ, Kramer MC, Gosai SJ, Yu X, Vandivier LE, Nelson ADL, Anderson ZD,**
676 **Beilstein MA, Fray RG, Lyons E, et al** (2018) N6-Methyladenosine Inhibits Local
677 Ribonucleolytic Cleavage to Stabilize mRNAs in Arabidopsis. Cell Rep **25**: 1146-
678 1157.e3
679 **Bai B, Peviani A, van der Horst S, Gamm M, Snel B, Bentsink L, Hanson J** (2017)
680 Extensive translational regulation during seed germination revealed by polysomal
681 profiling. New Phytol **214**: 233–244
682 **Franke KR, Schmidt SA, Park S, Jeong DH, Accerbi M, Green PJ** (2018) Analysis of
683 Brachypodium miRNA targets: Evidence for diverse control during stress and
684 conservation in bioenergy crops. BMC Genomics **19**: 1–18
685 **Garre E, Pelechano V, Sánchez del Pino M, Alepuz P, Sunnerhagen P** (2018) The Lsm1-
686 7/Pat1 complex binds to stress-activated mRNAs and modulates the response to
687 hyperosmotic shock. PLoS Genet **14**: 1–30
688 **German MA, Pillay M, Jeong DH, Hetawal A, Luo S, Janardhanan P, Kannan V,**
689 **Rymarquis LA, Nobuta K, German R, et al** (2008) Global identification of
690 microRNA-target RNA pairs by parallel analysis of RNA ends. Nat Biotechnol **26**: 941–
691 946
692 **Heck AM, Wilusz J** (2018) The interplay between the RNA decay and translation machinery
693 in eukaryotes. Cold Spring Harb Perspect Biol. doi: 10.1101/cshperspect.a032839
694 **Hou C, Lee W, Chou H, Chen A, Chou S, Chen H** (2016) Global Analysis of Truncated
695 RNA Ends Reveals New Insights into Ribosome Stalling in Plants. Plant Cell **28**: 2398–
696 2416
697 **Hou CY, Wu MT, Lu SH, Hsing YI, Chen HM** (2014) Beyond cleaved small RNA targets:
698 Unraveling the complexity of plant RNA degradome data. BMC Genomics. doi:
699 10.1186/1471-2164-15-15
700 **Hu W, Petzold C, Coller J, Baker KE** (2010) Nonsense-mediated mRNA decapping occurs
701 on polyribosomes in Saccharomyces cerevisiae. Nat Struct Mol Biol **17**: 244–247
702 **Hu W, Sweet TJ, Chamnongpol S, Baker KE, Coller J** (2009) Co-translational mRNA
703 decay in Saccharomyces cerevisiae. Nature **461**: 225–229
704 **Huang DW, Sherman BT, Lempicki RA** (2009) Systematic and integrative analysis of large

gene lists using DAVID bioinformatics resources. Nat Protoc **4**: 44–57

Ibrahim F, Maragkakis M, Alexiou P, Mourelatos Z (2018) Ribothrypsis, a novel process of canonical mRNA decay, mediates ribosome-phased mRNA endonucleolysis. Nat Struct Mol Biol **25**: 302–310

Ingolia NT, Ghaemmaghami S, Newman JRS, Weissman JS (2009) Genome-wide analysis in vivo of translation with nucleotide resolution using ribosome profiling. Science (80-) **324**: 218–223

Johnson AW (1997) Rat1p and Xrn1p are functionally interchangeable exoribonucleases that are restricted to and required in the nucleus and cytoplasm, respectively. Mol Cell Biol **17**: 6122–6130

Kawa D, Meyer AJ, Dekker HL, Abd-El-Haliem AM, Gevaert K, Van De Slijke E, Maszkowska J, Bucholc M, Dobrowolska G, De Jaeger G, et al (2020) SnRK2 Protein Kinases and mRNA Decapping Machinery Control Root Development and Response to Salt. Plant Physiol **182**: 361–377

Lee W, Hou B, Hou C, Tsao S, Kao P, Chen H, Biotechnology A (2020) Widespread Exon Junction Complex Footprints in the RNA Degradome Mark mRNA Degradation Before Steady-state Translation. doi: 10.1105/tpc.19.00666

Lin Z, Gasic I, Chandrasekaran V, Peters N, Shao S, Mitchison TJ, Hegde RS (2020) TTC5 mediates autoregulation of tubulin via mRNA degradation. Science **367**: 100–104

Love MI, Huber W, Anders S (2014) Moderated estimation of fold change and dispersion for RNA-seq data with DESeq2. Genome Biol **15**: 1–21

Merret R, Bousquet-Antonelli C (2020) Immunity gate-keepers. Nat Plants **6**: 608–609

Merret R, Descombin J, Juan Y ting, Favory JJ, Carpentier MC, Chaparro C, Charng Y yung, Deragon JM, Bousquet-Antonelli C (2013) XRN4 and LARP1 are required for a heat-triggered mRNA decay pathway involved in plant acclimation and survival during thermal stress. Cell Rep **5**: 1279–1293

Merret R, Nagarajan VK, Carpentier MC, Park S, Favory JJ, Descombin J, Picart C, Charng YY, Green PJ, Deragon JM, et al (2015) Heat-induced ribosome pausing triggers mRNA co-translational decay in Arabidopsis thaliana. Nucleic Acids Res **43**: 4121–4132

Nagarajan VK, Kukulich PM, von Hagel B, Green PJ (2019) RNA degradomes reveal substrates and importance for dark and nitrogen stress responses of Arabidopsis XRN4. Nucleic Acids Res **47**: 9216–9230

Narsai R, Howell KA, Millar AH, O'Toole N, Small I, Whelan J (2007) Genome-wide

analysis of mRNA decay rates and their determinants in Arabidopsis thaliana. Plant Cell **19**: 3418–3436

Pelechano V, Wei W, Steinmetz LM (2015) Widespread co-translational RNA decay reveals ribosome dynamics. Cell **161**: 1400–1412

Potuschak T, Vansiri A, Binder BM, Lechner E, Vierstra RD, Genschik P (2006) The exoribonuclease XRN4 is a component of the ethylene response pathway in Arabidopsis. Plant Cell **18**: 3047–3057

Presnyak V, Alhusaini N, Chen YH, Martin S, Morris N, Kline N, Olson S, Weinberg D, Baker KE, Graveley BR, et al (2015) Codon optimality is a major determinant of mRNA stability. Cell **160**: 1111–1124

Radhakrishnan A, Chen YH, Martin S, Alhusaini N, Green R, Coller J (2016) The DEAD-Box Protein Dhh1p Couples mRNA Decay and Translation by Monitoring Codon Optimality. Cell **167**: 122-132.e9

Reynoso MA, Juntawong P, Lancia M, Blanco FA, Bailey-Serres J, Zanetti ME (2015) Translating Ribosome Affinity Purification (TRAP) Followed by RNA Sequencing Technology (TRAP-SEQ) for Quantitative Assessment of Plant Translatomes. Methods Mol Biol **1284**: 185–207

Simms CL, Yan LL, Zaher HS (2017) Ribosome Collision Is Critical for Quality Control during No-Go Decay. Mol Cell **68**: 361-373.e5

Sorenson RS, Deshotel MJ, Johnson K, Adler FR, Sieburth LE (2018) Arabidopsis mRNA decay landscape arises from specialized RNA decay substrates, decapping-mediated feedback, and redundancy . Proc Natl Acad Sci **115**: E1485–E1494

Souret FF, Kastenmayer JP, Green PJ (2004) AtXRN4 degrades mRNA in Arabidopsis and its substrates include selected miRNA targets. Mol Cell **15**: 173–183

Tuck AC, Rankova A, Arpat AB, Liechti LA, Hess D, Iesmantavicius V, Castelo-Szekely V, Gatfield D, Bühler M (2020) Mammalian RNA Decay Pathways Are Highly Specialized and Widely Linked to Translation. Mol Cell **77**: 1222-1236.e13

Wawer I, Golisz A, Sulkowska A, Kawa D, Kulik A, Kufel J (2018) mRNA decapping and 5′-3′ decay contribute to the regulation of ABA signaling in Arabidopsis thaliana. Front Plant Sci **9**: 1–12

Willmann MR, Berkowitz ND, Gregory BD (2014) Improved genome-wide mapping of uncapped and cleaved transcripts in eukaryotes-GMUCT 2.0. Methods **67**: 64–73

Windels D, Bucher E (2018) The 5′-3′ exoribonuclease XRN4 regulates auxin response via the degradation of auxin receptor transcripts. Genes (Basel). doi: 10.3390/genes9120638

Yu X, Willmann MR, Anderson SJ, Gregory BD (2016) Genome-Wide Mapping of Uncapped and Cleaved Transcripts Reveals a Role for the Nuclear mRNA Cap-Binding Complex in Cotranslational RNA Decay in Arabidopsis. Plant Cell **28**: 2385–2397

Zhang W, Murphy C, Sieburth LE (2010) Conserved RNaseII domain protein functions in cytoplasmic mRNA decay and suppresses Arabidopsis decapping mutant phenotypes. Proc Natl Acad Sci U S A **107**: 15981–15985

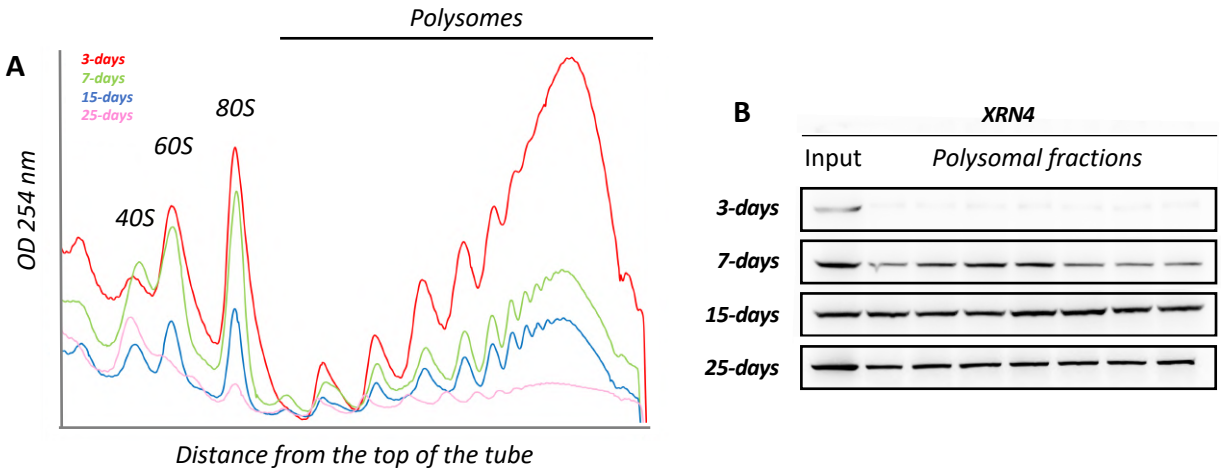

Figure 1 : XRN4 differentially accumulates in polysomes across seedling development. A. Polysomal extracts prepared from 3-, 7-, 15- and 25-d-old seedlings were fractionated on a sucrose gradient and polysome traces obtained through measurement of OD_{254nm}. Polysome profiling were performed starting from identical quantities of N_2-pulverized tissues (e.g 300 mg of biomass). **B.** Total proteins extracted from polysomal and input fractions were analyzed by western blotting. The four blots were probed with an antibody specific to XRN4. Inputs correspond to an equivalent of 10 mg of tissue powder for all stages. For polysomal fraction, loaded proteins were precipitated from identical volumes of each fraction. Data are representative of at least three replicates.

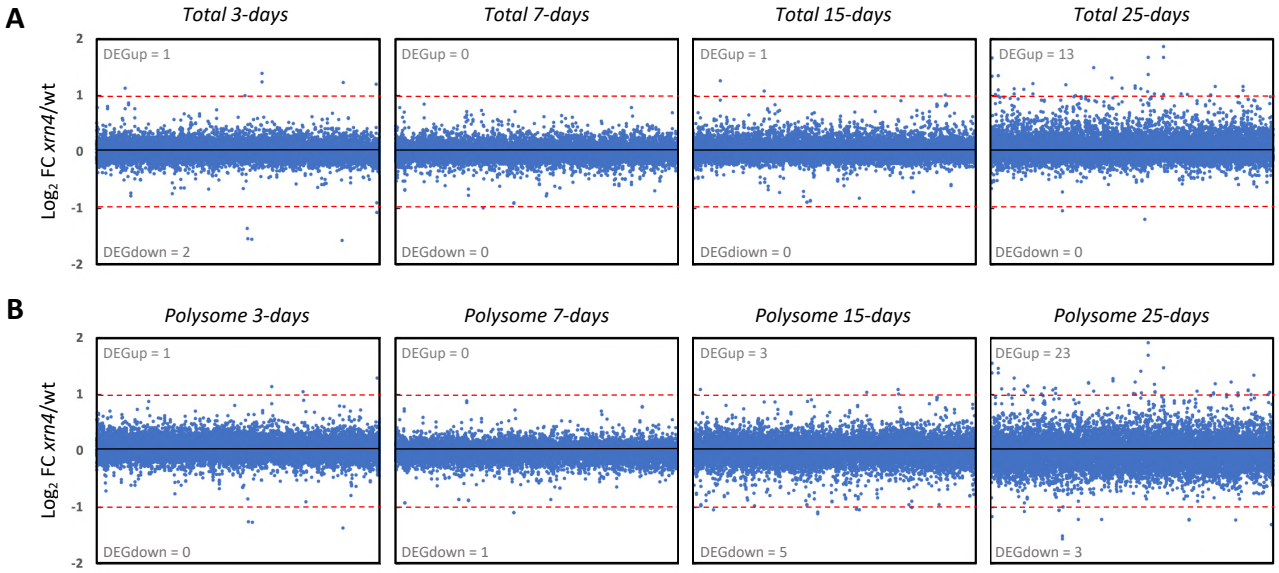

Figure 2 : XRN4 loss-of-function has low impact across seedling development at total (A) and polysome (B) RNA levels. Fold changes between *xrn4-5* and Col0 (wt) were calculated for each transcript in each condition. The $\log_2$ value of the mean is represented in each graph. The number of transcripts significantly mis-regulated in *xrn4-5* is reported and was calculated using DESeq2. Dashed red lines mark the $|\log_2 (2)|$ values.

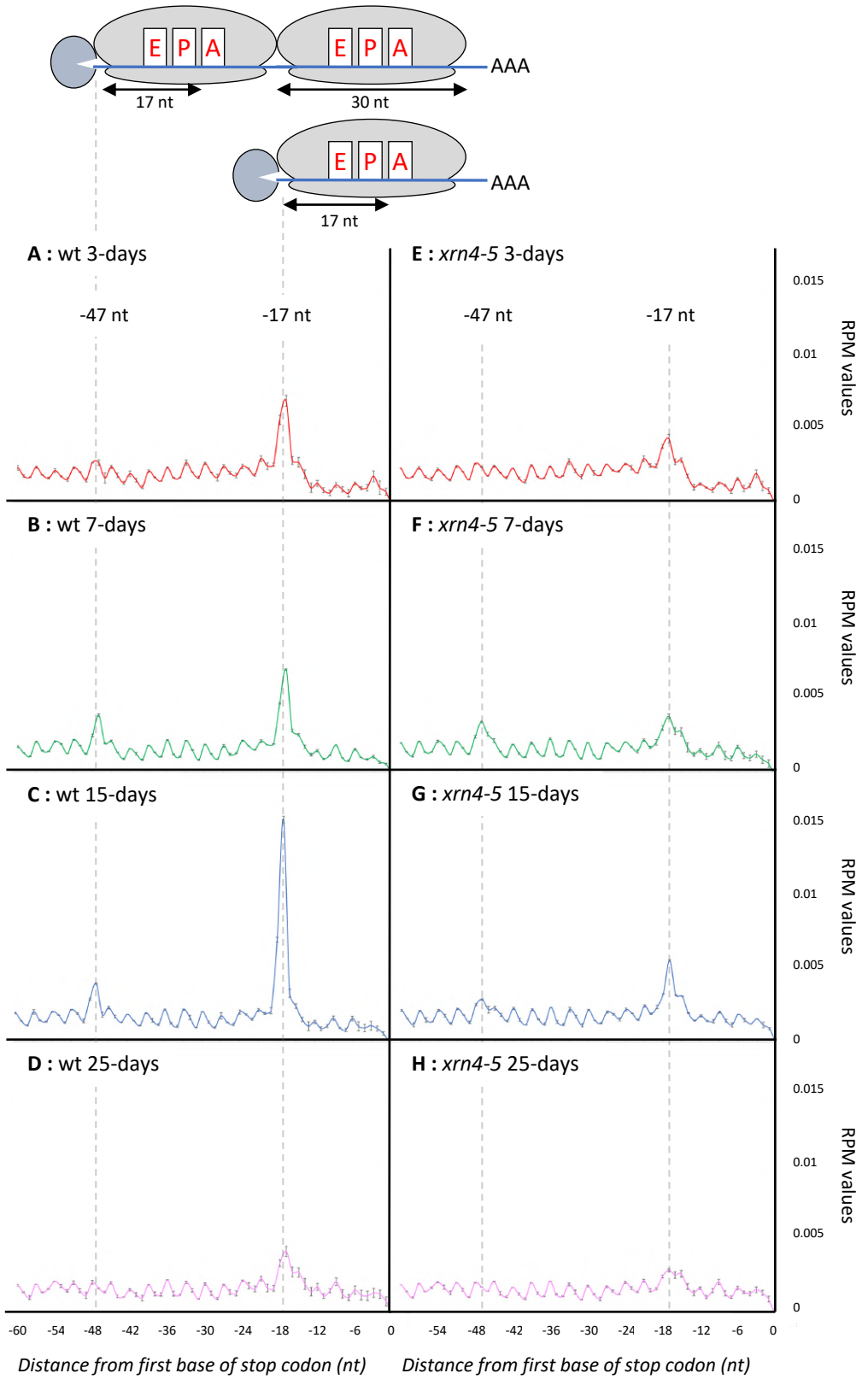

Figure 3 : Metagene analyses displaying the abundance of 5'P reads relative to stop codons. A. wt 3-d-old stage, **B.** wt 7-d-old stage, **C.** wt 15-d-old stage, **D.** wt 25-d-old stage, **E.** *xrn4-5* 3-d-old stage, **F.** *xrn4-5* 7-d-old stage, **G.** *xrn4-5* 15-d-old stage, **H.** *xrn4-5* 25-d-old stage. Mean ± SD. The illustrations represent 5'P intermediates accumulation at - 47 nt and - 17 nt before stop codons.

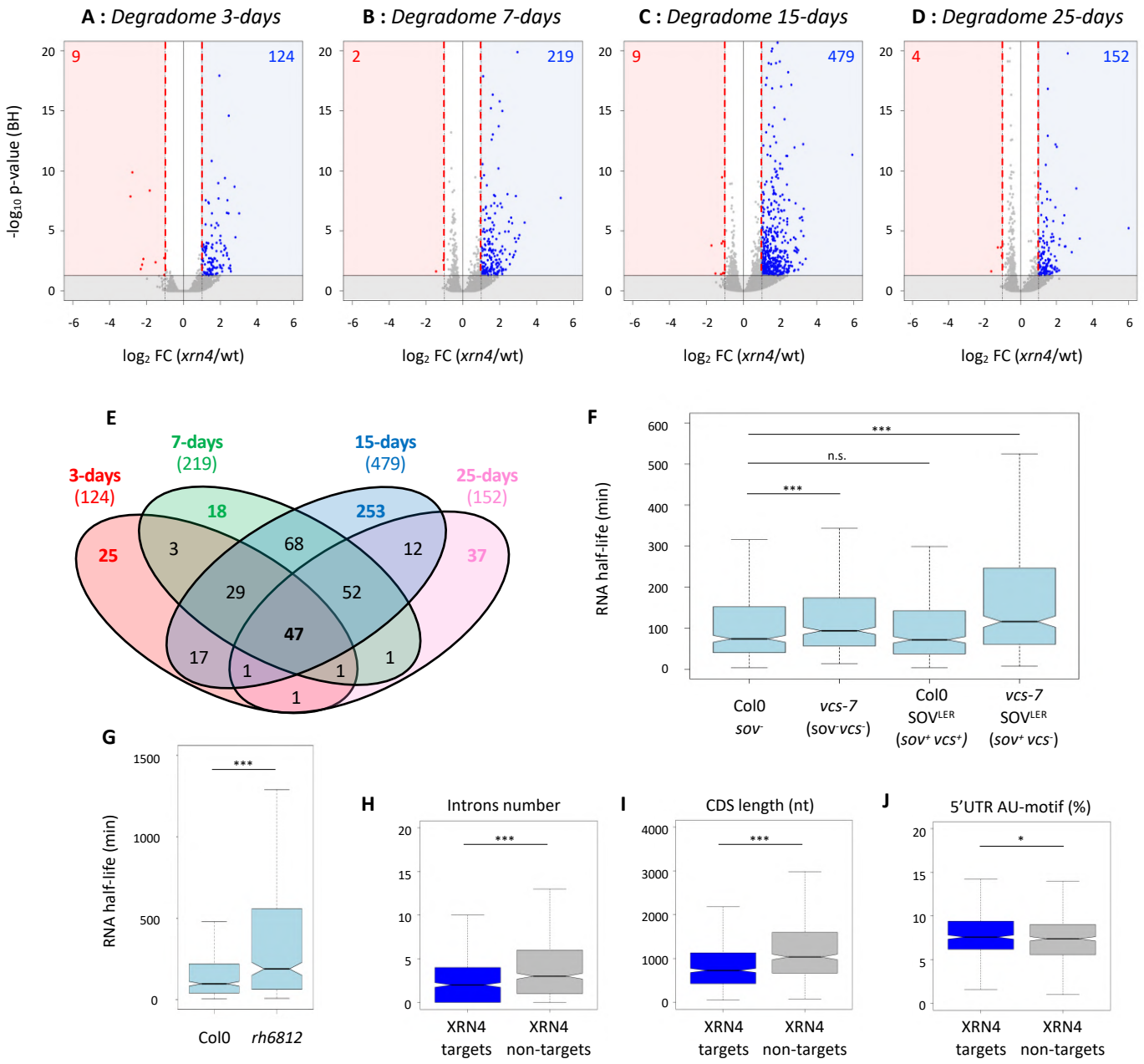

Figure 4 : Identification and features of XRN4 co-translational decay targets across development. A-D. Volcano plot of the change in read abundance in *xrn4-5* over wt (Col0). Vertical red dotted lines mark the $|\log_2(2)|$ values. Log_2 fold change and Benjamini-Hochberg adjusted p-values (BH) were calculated through the DESeq2 pipeline (as DEG in blue for up-regulated and red for down-regulated transcripts). Horizontal plain black lines demarcate adjusted p-values of 0.05. **E.** Venn diagram of co-translational decay targets across development. **F-G.** Majority of XRN4 co-translational decay targets show longer RNA half-life in *vcs-7, vcs-7* SOV^{LER} mutants (F) and *rh6812* mutant (G). RNA half-lives were collected from Sorenson et al., 2019 (F) or from Chantarachot et al., 2020 (G). Only transcripts present in each dataset are represented (N = 444/565 for F or N = 390/565 for G). **H-J.** Introns number, CDS length, and proportion of AU-motif in 5'UTR respectively of transcripts targeted by XRN4 compared to non-targeted random transcripts. N=565. *** p-values < 0.001, * p-values < 0.05, n.s. non significant.

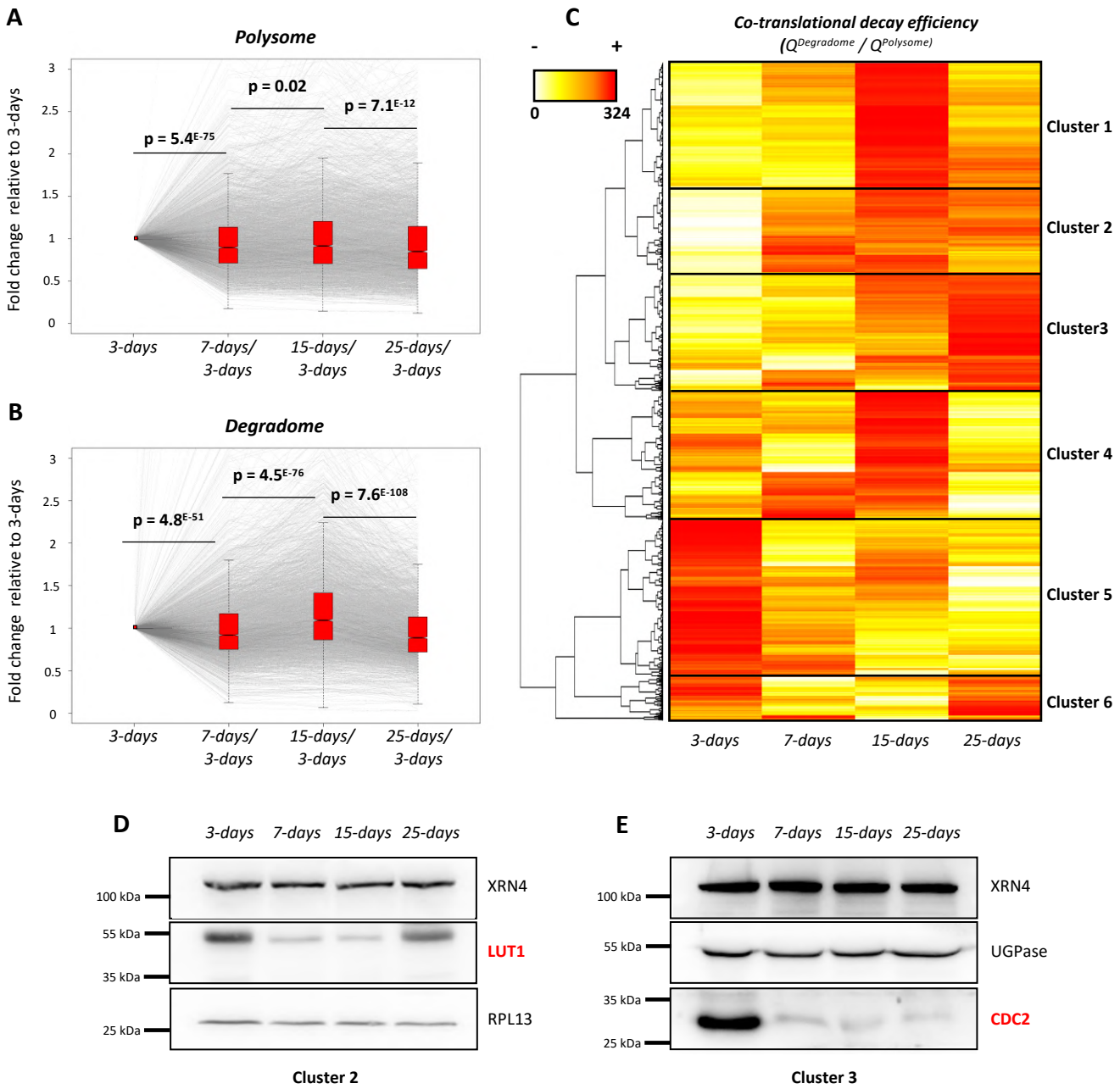

Figure 5: Co-translational decay is regulated across development and influences protein production. A. Transcript variation at polysome level across development using 3-days as a reference (N=3,366). **B.** Transcript variation at degradome level across development using 3-days as a reference (N=3,366). Gray lines represent individual transcript variation. Transcript distribution is represented by notched boxplots and significance was assessed by p-values (nonparametric Wilcoxon test). **C.** Heat Map of co-translational decay efficiency (ratio in degradome data over polysome RNAseq data) (N=3,366). Red values correspond to a high decay efficiency and yellow values to a low decay efficiency. **D, E.** Western blottings using LUT1 and CDC2 antibodies respectively. Both candidates were analyzed on distinct SDS-PAGE gels (8% and 10% acrylamide respectively). RPL13 and UGPase antibodies were used as loading controls. Each western blot was performed on two biological replicates.

Parsed Citations

Addo-Quaye C, Eshoo TW, Bartel DP, Axtell MJ (2008) Endogenous siRNA and miRNA Targets Identified by Sequencing of the Arabidopsis Degradome. Curr Biol 18: 758–762
Google Scholar: Author Only Title Only Author and Title

Anderson SJ, Kramer MC, Gosai SJ, Yu X, Vandivier LE, Nelson ADL, Anderson ZD, Beilstein MA, Fray RG, Lyons E, et al (2018) N6-Methyladenosine Inhibits Local Ribonucleolytic Cleavage to Stabilize mRNAs in Arabidopsis. Cell Rep 25: 1146-1157.e3
Google Scholar: Author Only Title Only Author and Title

Bai B, Peviani A, van der Horst S, Gamm M, Snel B, Bentsink L, Hanson J (2017) Extensive translational regulation during seed germination revealed by polysomal profiling. New Phytol 214: 233–244
Google Scholar: Author Only Title Only Author and Title

Franke KR, Schmidt SA, Park S, Jeong DH, Accerbi M, Green PJ (2018) Analysis of Brachypodium miRNA targets: Evidence for diverse control during stress and conservation in bioenergy crops. BMC Genomics 19: 1–18
Google Scholar: Author Only Title Only Author and Title

Garre E, Pelechano V, Sánchez del Pino M, Alepuz P, Sunnerhagen P (2018) The Lsm1-7/Pat1 complex binds to stress-activated mRNAs and modulates the response to hyperosmotic shock. PLoS Genet 14: 1–30
Google Scholar: Author Only Title Only Author and Title

German MA, Pillay M, Jeong DH, Hetawal A, Luo S, Janardhanan P, Kannan V, Rymarquis LA, Nobuta K, German R, et al (2008) Global identification of microRNA-target RNA pairs by parallel analysis of RNA ends. Nat Biotechnol 26: 941–946
Google Scholar: Author Only Title Only Author and Title

Heck AM, Wilusz J (2018) The interplay between the RNA decay and translation machinery in eukaryotes. Cold Spring Harb Perspect Biol. doi: 10.1101/cshperspect.a032839
Google Scholar: Author Only Title Only Author and Title

Hou C, Lee W, Chou H, Chen A, Chou S, Chen H (2016) Global Analysis of Truncated RNA Ends Reveals New Insights into Ribosome Stalling in Plants. Plant Cell 28: 2398–2416
Google Scholar: Author Only Title Only Author and Title

Hou CY, Wu MT, Lu SH, Hsing YI, Chen HM (2014) Beyond cleaved small RNA targets: Unraveling the complexity of plant RNA degradome data. BMC Genomics. doi: 10.1186/1471-2164-15-15
Google Scholar: Author Only Title Only Author and Title

Hu W, Petzold C, Coller J, Baker KE (2010) Nonsense-mediated mRNA decapping occurs on polyribosomes in Saccharomyces cerevisiae. Nat Struct Mol Biol 17: 244–247
Google Scholar: Author Only Title Only Author and Title

Hu W, Sweet TJ, Chamnongpol S, Baker KE, Coller J (2009) Co-translational mRNA decay in Saccharomyces cerevisiae. Nature 461: 225–229
Google Scholar: Author Only Title Only Author and Title

Huang DW, Sherman BT, Lempicki RA (2009) Systematic and integrative analysis of large gene lists using DAVID bioinformatics resources. Nat Protoc 4: 44–57
Google Scholar: Author Only Title Only Author and Title

Ibrahim F, Maragkakis M, Alexiou P, Mourelatos Z (2018) Ribothrypsis, a novel process of canonical mRNA decay, mediates ribosome-phased mRNA endonucleolysis. Nat Struct Mol Biol 25: 302–310
Google Scholar: Author Only Title Only Author and Title

Ingolia NT, Ghaemmaghami S, Newman JRS, Weissman JS (2009) Genome-wide analysis in vivo of translation with nucleotide resolution using ribosome profiling. Science (80-) 324: 218–223
Google Scholar: Author Only Title Only Author and Title

Johnson AW (1997) Rat1p and Xrn1p are functionally interchangeable exoribonucleases that are restricted to and required in the nucleus and cytoplasm, respectively. Mol Cell Biol 17: 6122–6130
Google Scholar: Author Only Title Only Author and Title

Kawa D, Meyer AJ, Dekker HL, Abd-El-Haliem AM, Gevaert K, Van De Slijke E, Maszkowska J, Bucholc M, Dobrowolska G, De Jaeger G, et al (2020) SnRK2 Protein Kinases and mRNA Decapping Machinery Control Root Development and Response to Salt. Plant Physiol 182: 361–377
Google Scholar: Author Only Title Only Author and Title

Lee W, Hou B, Hou C, Tsao S, Kao P, Chen H, Biotechnology A (2020) Widespread Exon Junction Complex Footprints in the RNA Degradome Mark mRNA Degradation Before Steady-state Translation. doi: 10.1105/tpc.19.00666
Google Scholar: Author Only Title Only Author and Title

Lin Z, Gasic I, Chandrasekaran V, Peters N, Shao S, Mitchison TJ, Hegde RS (2020) TTC5 mediates autoregulation of tubulin via mRNA degradation. Science 367: 100–104

Google Scholar: Author Only Title Only Author and Title

Love MI, Huber W, Anders S (2014) Moderated estimation of fold change and dispersion for RNA-seq data with DESeq2. Genome Biol 15: 1–21
Google Scholar: Author Only Title Only Author and Title

Merret R, Bousquet-Antonelli C (2020) Immunity gate-keepers. Nat Plants 6: 608–609
Google Scholar: Author Only Title Only Author and Title

Merret R, Descombin J, Juan Y ting, Favory JJ, Carpentier MC, Chaparro C, Charng Y yung, Deragon JM, Bousquet-Antonelli C (2013) XRN4 and LARP1 are required for a heat-triggered mRNA decay pathway involved in plant acclimation and survival during thermal stress. Cell Rep 5: 1279–1293
Google Scholar: Author Only Title Only Author and Title

Merret R, Nagarajan VK, Carpentier MC, Park S, Favory JJ, Descombin J, Picart C, Charng YY, Green PJ, Deragon JM, et al (2015) Heat-induced ribosome pausing triggers mRNA co-translational decay in Arabidopsis thaliana. Nucleic Acids Res 43: 4121–4132
Google Scholar: Author Only Title Only Author and Title

Nagarajan VK, Kukulich PM, von Hagel B, Green PJ (2019) RNA degradomes reveal substrates and importance for dark and nitrogen stress responses of Arabidopsis XRN4. Nucleic Acids Res 47: 9216–9230
Google Scholar: Author Only Title Only Author and Title

Narsai R, Howell KA, Millar AH, O'Toole N, Small I, Whelan J (2007) Genome-wide analysis of mRNA decay rates and their determinants in Arabidopsis thaliana. Plant Cell 19: 3418–3436
Google Scholar: Author Only Title Only Author and Title

Pelechano V, Wei W, Steinmetz LM (2015) Widespread co-translational RNA decay reveals ribosome dynamics. Cell 161: 1400–1412
Google Scholar: Author Only Title Only Author and Title

Potuschak T, Vansiri A, Binder BM, Lechner E, Vierstra RD, Genschik P (2006) The exoribonuclease XRN4 is a component of the ethylene response pathway in Arabidopsis. Plant Cell 18: 3047–3057
Google Scholar: Author Only Title Only Author and Title

Presnyak V, Alhusaini N, Chen YH, Martin S, Morris N, Kline N, Olson S, Weinberg D, Baker KE, Graveley BR, et al (2015) Codon optimality is a major determinant of mRNA stability. Cell 160: 1111–1124
Google Scholar: Author Only Title Only Author and Title

Radhakrishnan A, Chen YH, Martin S, Alhusaini N, Green R, Coller J (2016) The DEAD-Box Protein Dhh1p Couples mRNA Decay and Translation by Monitoring Codon Optimality. Cell 167: 122-132.e9
Google Scholar: Author Only Title Only Author and Title

Reynoso MA, Juntawong P, Lancia M, Blanco FA, Bailey-Serres J, Zanetti ME (2015) Translating Ribosome Affinity Purification (TRAP) Followed by RNA Sequencing Technology (TRAP-SEQ) for Quantitative Assessment of Plant Translatomes. Methods Mol Biol 1284: 185–207
Google Scholar: Author Only Title Only Author and Title

Simms CL, Yan LL, Zaher HS (2017) Ribosome Collision Is Critical for Quality Control during No-Go Decay. Mol Cell 68: 361-373.e5
Google Scholar: Author Only Title Only Author and Title

Sorenson RS, Deshotel MJ, Johnson K, Adler FR, Sieburth LE (2018) Arabidopsis mRNA decay landscape arises from specialized RNA decay substrates, decapping-mediated feedback, and redundancy . Proc Natl Acad Sci 115: E1485–E1494
Google Scholar: Author Only Title Only Author and Title

Souret FF, Kastenmayer JP, Green PJ (2004) AtXRN4 degrades mRNA in Arabidopsis and its substrates include selected miRNA targets. Mol Cell 15: 173–183
Google Scholar: Author Only Title Only Author and Title

Tuck AC, Rankova A, Arpat AB, Liechti LA, Hess D, Iesmantavicius V, Castelo-Szekely V, Gatfield D, Bühler M (2020) Mammalian RNA Decay Pathways Are Highly Specialized and Widely Linked to Translation. Mol Cell 77: 1222-1236.e13
Google Scholar: Author Only Title Only Author and Title

Wawer I, Golisz A, Sulkowska A, Kawa D, Kulik A, Kufel J (2018) mRNA decapping and 5′-3′ decay contribute to the regulation of ABA signaling in Arabidopsis thaliana. Front Plant Sci 9: 1–12
Google Scholar: Author Only Title Only Author and Title

Willmann MR, Berkowitz ND, Gregory BD (2014) Improved genome-wide mapping of uncapped and cleaved transcripts in eukaryotes-GMUCT 2.0. Methods 67: 64–73
Google Scholar: Author Only Title Only Author and Title

Windels D, Bucher E (2018) The 5′-3′ exoribonuclease XRN4 regulates auxin response via the degradation of auxin receptor transcripts. Genes (Basel). doi: 10.3390/genes9120638
Google Scholar: Author Only Title Only Author and Title

Yu X, Willmann MR, Anderson SJ, Gregory BD (2016) Genome-Wide Mapping of Uncapped and Cleaved Transcripts Reveals a Role for

the Nuclear mRNA Cap-Binding Complex in Cotranslational RNA Decay in Arabidopsis. Plant Cell 28: 2385–2397
Google Scholar: Author Only Title Only Author and Title

Zhang W, Murphy C, Sieburth LE (2010) Conserved RNaseII domain protein functions in cytoplasmic mRNA decay and suppresses Arabidopsis decapping mutant phenotypes. Proc Natl Acad Sci U S A 107: 15981–15985
Google Scholar: Author Only Title Only Author and Title